Acta Cryst. (1991). A47, 686-698

Multiple Inelastic Scattering in High-Energy Electron Diffraction and Imaging

BY Z. L. WANG*

Metals and Ceramics Division, Oak Ridge National Laboratory, PO Box 2008, Oak Ridge, TN 37831-6376, USA, and Department of Materials Science and Engineering, The University of Tennessee, Knoxville, TN 37996-2200, USA

(*Received* 13 *December* 1990; *accepted* 7 *May* 1991)

Abstract

A dynamical multiple elastic and inelastic electron scattering theory is proposed and is applied to the plural scattering cases of phonon, single-electron and valence (or plasmon) excitations. The incoherence of all the possible inelastic scattering processes of different energies and momenta is evaluated analytically before any numerical calculations. The effects of multiple scattering are equivalent partially to the broadening of the scattering function of a single inelastic process by those of others and partially to the re-scattering of the Kikuchi pattern produced in one inelastic process by others. The final diffraction pattern is a convoluted result of those Kikuchi patterns produced by different inelastic scattering processes. All these characteristics can be considered in just one single formula. The theory of multiple-phonon excitations in simulating high-angle annular-dark-field (ADF) scanning transmission electron-microscopy (STEM) images is proposed. It is shown that the single-phonon scattering model is a good approximation except at the points close to atomic nuclei if the electron probe is comparable in size to that of an atom. The higher-order phonon scattering may improve the resolution of the ADF STEM images of thin crystals.

1. Introduction

Inelastic electron diffraction and imaging are important in characterizing crystal atomic structures. The fundamental theory describing inelastic electron scattering in a crystal was given by Yoshioka (1957). By considering the incident electron and the electrons in the crystal as a whole system, he derived a set of coupled Schrödinger equations that included the transitions between the ground state and the excited states of the crystal. Electron multiple elastic and inelastic scattering are included in these equations. Applications of this theory and other theories for single inelastic scattering have been made by many authors in various cases (Howie, 1963; Whelan, 1965*a*, *b*; Gjønnes, 1966; Gjønnes & Watanabe, 1966; Cowley & Pogany, 1968; Doyle, 1969; Humphreys & Whelan, 1969; Radi, 1970; Okamoto, Ichinokawa & Ohtsuki, 1971; Høier, 1973; Rez, Humphreys & Whelan, 1977; Maslen & Rossouw, 1984; Rossouw & Bursill, 1985; Bird & Wright, 1989; Wang, 1989, 1990). Since the lifetime of an excited state (typically 10^{-15} to 10^{-13} s) is much longer than the interaction time of a fast electron (100 keV) with an atom (about 10^{-18} s), the inelastic scattering of high-energy electrons can be treated as a time-independent process. The inclusion of the excited-state decay effect may be considered with the density matrix theory (Dudarev & Ryazanov, 1988).

Electron multiple inelastic scattering, as a small effect, may become important in exploring new microscopy techniques in the future because the energy-filtered diffraction patterns (Reimer & Fromm, 1989), for example, may contain the contributions of phonon double-scattered electrons. Although multiple inelastic scattering can be treated, in principle, by the Bloch-wave theory (Howie, 1963) and the multislice theory (Wang, 1989), the incoherence of different inelastic excited states makes it impractical to calculate the diffraction patterns formed by the electrons after exciting the states of different energies and momenta because the excitation of each state has to be calculated separately. Thermal diffuse scattering (TDS) or phonon scattering is such an example.

High-energy (typically 100 keV) electrons pass through specimens so rapidly that vibrating atoms are seen as if stationary. The electron diffraction pattern and image are the sums of the intensities for the many instantaneous pictures of displaced atoms. In other words, thermal diffuse scattering is actually a statistically averaged quasi-elastic scattering (energy loss $<0{\cdot}2$ eV) of the electrons from the crystal with different thermal-vibration configurations. Thus the final detected intensity distribution is a summation of all the possible *elastic* scattering from these different distorted lattices. This is the 'frozen' lattice model of TDS in electron diffraction (Hall, 1965; Hall & Hirsch, 1965; Fanidis, Van Dyck, Coene & Van Landuyt, 1989; Fanidis, Van Dyck & Van Landuyt, 1990; Wang & Cowley, 1990; Loane, Xu & Silcox,

* Send correspondence to Z. L. Wang, Metals and Ceramics Division, Oak Ridge National Laboratory, Bldg 5500, MS 6376, PO Box 2008, Oak Ridge, TN 37831-6376, USA.

0108-7673/91/060686-13$03.00

1991). However, it is impractical to repeat the whole calculation for large amounts of differently distorted crystal structures. Thus an important question in simulating TDS is how to take the statistical average of the elastic electron scattering from these lattice configurations before the numerical calculations.

This problem can be solved using the new dynamical theory recently proposed by Wang & Bentley (1990, 1991*a*). The phase correlations of the localized inelastic scattering occurring at different atomic sites can be statistically evaluated before any numerical calculations, essentially providing an easy way for treating coherence, incoherence or partial coherence in dynamical electron diffraction. The time average of electron diffraction from the lattices of different thermal vibration configurations can be performed in just a single calculation.

In this paper, the inelastic scattering theory proposed previously (Wang & Bentley, 1990, 1991*a*; Wang, 1991) will be further developed to treat multiple inelastic electron scattering in crystals. A theoretical scheme for double-scattering processes is given and is applied to double-phonon, double single-electron, phonon–single-electron and plasmon excitations (§ 3). This double inelastic scattering theory is generalized to multiple scattering cases in § 4. Finally, the effects of multiple phonon scattering in simulation of high-angle annular-dark-field (ADF) scanning transmission electron microscopy (STEM) images are described (§ 5).

2. The basic theory of electron inelastic scattering

The basic equations governing inelastic electron scattering in a crystal were derived from wave mechanics (Yoshioka, 1957). Consider the interaction of an incident electron with a solid; the Schrödinger equation of the system is

$$[-\hbar^2/2m_e\nabla^2 + H_c + H']\Phi = E\Phi, \qquad (1)$$

where $-(\hbar^2/2m_e)\nabla^2$ is the kinetic energy of the electron; $m_e = m_0/[1-(v/c)^2]^{1/2}$ is the mass of a moving electron with velocity v; $E = eV_0 + e^2V_0^2/2m_ec^2$; V_0 is the accelerating voltage of the electron microscope (Spence, 1988); H_c is the crystal Hamiltonian; H' describes the interaction between the electron and the solid. The wave function of the system, $\Phi(\mathbf{r}, \mathbf{r}_1, \ldots, \mathbf{r}_M)$, depends on the coordinates of the incident electron $\mathbf{r}$ and on the coordinates of the electrons and ions $\mathbf{r}_1, \ldots, \mathbf{r}_M$ of the crystal. Neglecting exchange effects, one can write

$$\Phi(\mathbf{r}, \mathbf{r}_1, \ldots, \mathbf{r}_M) = \sum_n a_n(\mathbf{r}_1, \ldots, \mathbf{r}_M)\Psi_n(\mathbf{r}), \qquad (2)$$

where a_n is the wave function of the crystal in its nth excited state of energy, ε_n, so that

$$H_c a_n = \varepsilon_n a_n. \qquad (3)$$

Ψ_0 in (2) describes the elastically scattered wave of energy $E_0 = E$ and Ψ_n describes the inelastically scattered wave of energy $E_n = E - \varepsilon_n$, with $n = 1, 2, \ldots$. Substitution of (2) and (3) into (1), multiplication by a_n^* and integrating over the coordinates $\mathbf{r}_1, \ldots, \mathbf{r}_M$ yields

$$(\nabla^2 + k_n^2)\Psi_n = (2m_e/\hbar^2)\sum_m H'_{nm}(\mathbf{r})\Psi_m \quad \text{with } n = 0, 1, 2, \ldots, \qquad (4a)$$

where

$$k_n^2 \equiv (2m_e/\hbar^2)E_n \qquad (4b)$$

and

$$H'_{nm} \equiv \int a_n^* H' a_m \, d\mathbf{r}_1, \ldots, d\mathbf{r}_M. \qquad (4c)$$

Multiple elastic and inelastic scattering of electrons in a crystal are all included in Yoshioka's coupled equations. If one assumes electron scattering angles are of the same magnitude as Bragg angles and takes the inelastic scattering as a position modulation to the inelastic incidence wave (*i.e.* the wave with energy E_n and wave vector $\mathbf{k}_n$), analogous to Howie's (1963) method, the solution of (4*a*) can be written in the form

$$\Psi_n \equiv \phi_n(\mathbf{r})\Psi_n^0(\mathbf{r}), \qquad (5a)$$

where $\Psi_n^0(\mathbf{r})$ is the elastic wave of free-space wave vector $\mathbf{k}_n$, which satisfies the boundary conditions and the elastic scattering Schrödinger equation

$$(\nabla^2 + k_n^2)\Psi_n^0 = (2m_e/\hbar^2)V(\mathbf{r})\Psi_n^0, \qquad (5b)$$

where $V = H'_{nn}$. It is important to point out that $\Psi_n^0(\mathbf{r})$ is the full solution of (5*b*) rather than a single stream of Bloch-wave solution. Therefore, (5*a*) has a more generalized meaning compared to that defined by Howie (1963). Equation (5*b*) can be solved using the multislice method for a known incident electron probe (Cowley & Moodie, 1957). Now one tries to seek the first-order solution of (4). Under the small-angle approximation, by neglecting the $\nabla^2\phi_n$ term and using (5*b*), (4*a*) becomes

$$\frac{\partial\Psi_n^0(\mathbf{r})}{\partial z}\frac{\partial\phi_n(\mathbf{r})}{\partial z} \simeq \alpha \sum_{m\neq n} H'_{nm}(\mathbf{r})\Psi_m^0(\mathbf{r})\phi_m(\mathbf{r}) \quad \text{with } n = 0, 1, 2, \ldots, \qquad (6)$$

where $\alpha \equiv m_e/\hbar^2$. Equation (6) can be rewritten as

$$\partial\phi_n(\mathbf{r})/\partial z = \alpha \sum_{m\neq n} U_{nm}(\mathbf{r})\phi_m(\mathbf{r}) \quad \text{with } n = 0, 1, 2, \ldots, \qquad (7a)$$

where

$$U_{nm} \equiv H'_{nm}(\mathbf{r})\Psi_m^0(\mathbf{r})[\partial\Psi_n^0(\mathbf{r})/\partial z]^{-1}. \qquad (7b)$$

For thin crystals satisfying $|\alpha\int_0^d dz\, U_{10}| \ll 1$ [*i.e.* $d \ll (\lambda/\pi)E/H'_{10}$, where λ is the electron wavelength],

and under the single-inelastic-scattering approximation,

$$\partial\phi_1(\mathbf{r})/\partial z = \alpha U_{10}(\mathbf{r})\phi_0(\mathbf{r}). \quad (8a)$$

The boundary condition is $\phi_1(\mathbf{b}, z=0)=0$, where $\mathbf{b}=(x, y)$. If the absorption effects of the inelastic scattering are neglected, $\phi_0(\mathbf{r})\simeq 1$ and one has

$$\phi_1(\mathbf{r}) \simeq \alpha \int_0^z \mathrm{d}z_1\, U_{10}(\mathbf{b}, z_1) \quad (8b)$$

or

$$\Psi_1(\mathbf{b}, z) = \alpha\left[\int_0^z \mathrm{d}z_1\, U_{10}(\mathbf{b}, z_1)\right]\Psi_n^0(\mathbf{b}, z). \quad (8c)$$

Equation (8*c*) is the first-order solution of (4*a*) for thin crystals under the single-inelastic-scattering approximation and is equivalent to the inelastic scattering multislice theory proposed by several authors (Cowly & Pogany, 1968; Doyle, 1969; Wang, 1989) (see Appendix *A* for proof). This inversely confirms the validity of the approximations under which (6) and (7) were derived.

Compared to the Bloch-wave (Howie, 1963; Maslen & Rossouw, 1984) and multislice theories, the most important feature of this new approach [(8*c*)] is that the phase correlations of the inelastic scattering process occurring at different atomic sites can be evaluated *analytically* before any numerical calculations. This provides an easy way for evaluating coherent, incoherent or partially coherent scattering between different inelastic excited states. Equation (8*c*) has been applied to treat single-phonon excitations based on the semiclassical 'frozen-lattice' model (Wang & Bentley, 1991*a*) and the full lattice dynamics (Wang, 1991). The theoretical results have successfully interpreted the thermal diffuse streaks observed in electron diffraction patterns and their intensity profiles. Further applications of (8*c*) have provided a simple theory for considering the valence excitation effects in simulating high-resolution electron microscopy images (Wang & Bentley, 1991*b*). In this paper, we try to use (8*c*) as the first-order iteration solution of (7*a*) and apply them to treat multiple inelastic scattering in electron diffraction.

3. Double inelastic scattering

3.1. *General theory*

Now consider the cases of double inelastic scattering. The crystal can be considered as either in its ground state (elastic) or in one of its two 'independent' excited states. By independent one means that the excitation of each state is not affected by the other one and can be treated separately, such as single-electron and phonon excitations. The transitions from the ground state to each of the two states can be described by (8). If the transition-matrix elements are denoted by $U_{(1)}=U_{10}$ for $\phi_{(1)}$ and $U_{(2)}=U_{20}$ for $\phi_{(2)}$, the double scattering (ϕ_D) can only be either from process (or event) $\phi_{(1)}$ to process $\phi_{(2)}$ or from $\phi_{(2)}$ to $\phi_{(1)}$ (see Fig. 1*a*). This treatment has separated the double inelastic scattering into two single-step processes; the direct scattering (or one-step process) of the electrons from the ground state (ϕ_0) to the final inelastic state (ϕ_D) (such as the excitation of a double plasmon, for example) is neglected. This direct scattering is usually termed the 'coherent' inelastic scattering [for double-plasmon excitations see Spence & Spargo (1971)] and is typically small in practice. Thus, according to (7*a*), one has

$$\begin{aligned}\partial\phi_D(\mathbf{r})/\partial z &= \alpha\{U_{(2)}(\mathbf{r})\phi_{(1)}(\mathbf{r}) + U_{(1)}(\mathbf{r})\phi_{(2)}(\mathbf{r})\}\\ &= \alpha^2\Big\{U_{(2)}(\mathbf{r})\int_0^z \mathrm{d}z_1\, U_{(1)}(\mathbf{b}, z_1)\\ &\quad + U_{(1)}(\mathbf{r})\int_0^z \mathrm{d}z_1\, U_{(2)}(\mathbf{b}, z_1)\Big\}. \quad (9)\end{aligned}$$

In (9), the electrons which undergo inelastic event 1 first then event 2 or event 2 first then event 1 would have the same phase shift; thus they can be treated as coherent. The first term in (9) means the inelastically scattered wave generated at depth z_1 by event 1 is being inelastically scattered (event 2) again at depth z after being elastically scattered from z_1 to z. An equivalent interpretation applies to the second term. The solution of (9) is

$$\phi_D(\mathbf{r}) = \alpha^2\left\{\int_0^z \mathrm{d}z_1\, U_{(1)}(\mathbf{b}, z_1)\int_0^z \mathrm{d}z_1'\, U_{(2)}(\mathbf{b}, z_1')\right\}, \quad (10)$$

which satisfies the boundary condition $\phi_D(\mathbf{b}, z=0)=0$. If one puts (10) and (7*b*) into (5*a*), the double-

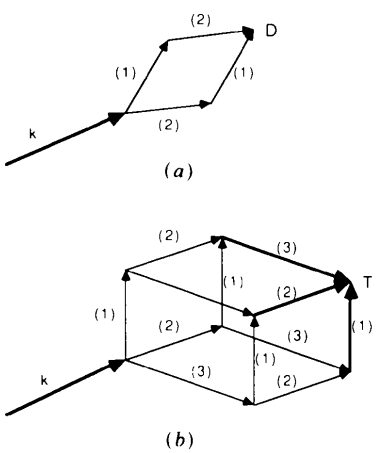

Fig. 1. Schematic models showing (*a*) double and (*b*) triple 'independent' inelastic-scattering processes in high-energy electron diffraction, where (n), $n=1, 2, \ldots$, means the nth inelastic-scattering process or event.

scattered wave at the exit face of the crystal $z = d$ is

$$\Psi_D(\mathbf{b}, d) = \alpha^2 \left\{ \int_0^d dz_1\, H'_{(1)}(\mathbf{b}, z_1, \mathbf{q}) S_{(1)}(\mathbf{b}, z_1) \times \int_0^d dz'_1\, H'_{(2)}(\mathbf{b}, z'_1, \mathbf{q}') S_{(2)}(\mathbf{b}, z'_1) \right\} \times \Psi^0_D(\mathbf{b}, d), \quad (11a)$$

where

$$S_{(n)}(\mathbf{b}, z) \equiv \Psi^0_0(\mathbf{b}, z)[\partial \Psi^0_{(n)}(\mathbf{b}, z)/\partial z]^{-1}. \quad (11b)$$

$\Psi^0_{(1)}$, $\Psi^0_{(2)}$ and Ψ^0_D are the elastically scattered waves of incident electrons of wave vector $\mathbf{k}_{(1)}$, $\mathbf{k}_{(2)}$ and $\mathbf{k}_D$, respectively, and $H'_{(1)}$ and $H'_{(2)}$ are the interaction Hamiltonians for process 1 (of momentum transfer $\mathbf{q}$) and 2 (of momentum transfer $\mathbf{q}'$), respectively. The calculation of $S_{(n)}$ in the multislice scheme is given in Appendix *B*. The physical meaning of (11*a*) can be simply stated as follows. The double inelastic waves can be generated at any point inside the specimen with a probability function proportional to $|H'_{(1)}H'_{(2)}|^2$. The inelastic events occurring at different atom locations are marked with a 'historical tag', $S_{(n)} = \Psi^0_0(\mathbf{r})[\partial \Psi^0_{(n)}(\mathbf{r})/\partial z]^{-1}$, which is responsible for the formation of Kikuchi lines (see Appendix *B*); the elastic scattering of those electrons after a single inelastic excitation is the same as the elastic scattering of incident electrons with equivalent energy and momentum. In practice, the determination of $\Psi^0_{(n)}$ for different momentum transfers (or different incident wave vectors) involves huge amounts of calculations. For simplification, one assumes that the inelastic scattering does not significantly affect the distribution of electron current inside the crystal, *i.e.* $\Psi^0_{(n)}(\tau, d) \simeq \Psi^0_0(\tau, d)$. Defining

$$X(\mathbf{b}, z_1, z'_1) = S_{(1)}(\mathbf{b}, z_1) S_{(2)}(\mathbf{b}, z'_1) \Psi^0_0(\mathbf{b}, d) \quad (12)$$

and taking a 2D Fourier transform of (11*a*), in reciprocal space $\tau = (\tau_x, \tau_y)$, one obtains

$$\Psi_D(\tau, d) \simeq \alpha^2 \int_0^d dz \int_0^d dz'\, H'_{(1)}(\tau, z, \mathbf{q}) \otimes H'_{(2)}(\tau, z', \mathbf{q}') \otimes X(\tau, z, z'), \quad (13)$$

where $\otimes$ indicates a convolution operation of τ. In general, for a 3D periodic crystal structure (Howie, 1963), H' can be written as

$$H'_{(n)}(\mathbf{r}, \mathbf{q}) = \exp(i\mathbf{q} \cdot \mathbf{r}) \sum_g H'^{(n)}_g(\mathbf{g} - \mathbf{q}) \exp(-i\mathbf{g} \cdot \mathbf{r}) \quad (14a)$$

or

$$H'_n(\tau, z, \mathbf{q}) = [(2\pi)^2/A] \exp(iq_z z) \times \sum_g H'^{(n)}_g(\mathbf{g} - \mathbf{q}) \delta(\tau - \mathbf{q} + \mathbf{q}_b), \quad (14b)$$

where $H'^{(n)}_g$ is the Fourier coefficient of the interaction matrix element H'_n, A is the area of the crystal unit cell perpendicular to the incident-beam direction and $\hbar\mathbf{q} = \hbar(\mathbf{k}_0 - \mathbf{k}_{(n)})$ is the momentum transferred by the incident electron. Putting (14*b*) into (13), one obtains

$$\begin{aligned} \Psi_D(\tau, d) &= (4\pi^2\alpha/A)^2 \int_0^d dz \int_0^d dz' \exp[i(q_z z + q'_z z')] \\ &\quad \times \sum_g \sum_{g'} H'^{(1)}_g H'^{(2)}_{g'} \\ &\quad \times X(\tau - \mathbf{g} + \mathbf{q}_b - \mathbf{g}' + \mathbf{q}'_b, z, z') \\ &= (4\pi^2\alpha/A)^2 \sum_g \sum_{g'} H'^{(1)}_g(\mathbf{g} - \mathbf{q})\, H'^{(2)}_{g'}(\mathbf{g}' - \mathbf{q}') \\ &\quad \times Z(\tau - \mathbf{g} + \mathbf{q}_b - \mathbf{g}' + \mathbf{q}'_b, q_z, q'_z), \end{aligned} \quad (15)$$

where

$$Z(\tau, q_z, q_{z'}) \equiv \left[\int_0^d dz \exp(iq_z z) S_{(1)}(\tau, z) \right] \otimes \left[\int_0^d dz' \exp(iq'_z z') S_{(2)}(\tau, z') \right] \otimes \Psi^0_0(\tau, d). \quad (16)$$

In (16), the convolution of $S_{(1)}$ with $S_{(2)}$ means the rescattering of the Kikuchi pattern produced in event 1 by the second inelastic event 2. Summing the intensities contributed by the inelastic scattering processes of different $\mathbf{q}$ and $\mathbf{q}'$s incoherently and neglecting the coupling between different $\mathbf{g}$'s, one obtains

$$\begin{aligned} I_D(\tau) &= [V_c/(2\pi)^3]^2 \int_{BZ} d\mathbf{q} \int_{BZ} d\mathbf{q}' \, |\Psi_D(\tau, d)|^2 \\ &\simeq [V_c/(2\pi)^3]^2 (4\pi^2\alpha/A)^4 \sum_g \sum_{g'} \int_{BZ} d\mathbf{q} \int_{BZ} d\mathbf{q}' \\ &\quad \times |H'^{(1)}_g(\mathbf{g} - \mathbf{q})|^2 |H'^{(2)}_{g'}(\mathbf{g}' - \mathbf{q}')|^2 \\ &\quad \times |Z(\tau - \mathbf{g} + \mathbf{q}_b - \mathbf{g}' + \mathbf{q}'_b, q_z, q'_z)|^2, \end{aligned} \quad (17)$$

where V_c is the volume of the unit cell; the integration of $\mathbf{q}$ and $\mathbf{q}'$ is restricted to the first Brillouin zone (BZ) and the subscript b refers to the projection of the corresponding quantity in the xy plane. Equation (17) can be further simplified by separating the integration of $\mathbf{q}$ into $\mathbf{q}_b = (q_x, q_y)$ and q_z. By defining a function

$$T^{(1)}_g(\mathbf{g} - \mathbf{q}_b) \equiv \begin{cases} (a_3/2\pi) \int_{BZ} dq_z |H'^{(1)}_g(\mathbf{g} - \mathbf{q})|^2 & \text{if } \mathbf{q}_b \text{ falls within the first BZ} \\ 0 & \text{otherwise} \end{cases} \quad (18)$$

where $a_3 = V_c/A$ is the height of the unit cell in the z direction, one can extend the integration of $\mathbf{q}_b$ to $(-\infty, \infty)$ in reciprocal space. Since q_z and q'_z are mainly related to the electron energy loss by $q_z \simeq k_0(E - E_1)/2E$ and $q'_z \simeq k_0(E - E_2)/2E$ independent of $\mathbf{q}_b$ and $\mathbf{q}'_b$ (Egerton, 1986), one can take $Z(\tau, q_z, q'_z) = Z(\tau)$ out of the integrations of q_z and

q_z' and thus

$$I_D(\tau) \simeq \xi^4 \sum_g \sum_{g'} \int_{-\infty}^{\infty} d\mathbf{q}_b \int_{-\infty}^{\infty} d\mathbf{q}_b' \, T_g^{(1)}(\mathbf{g}-\mathbf{q}_b) \times T_g^{(2)}(\mathbf{g}'-\mathbf{q}_b')|Z(\tau-\mathbf{g}+\mathbf{q}_b-\mathbf{g}'+\mathbf{q}_b')|^2$$

$$= \xi^4 \sum_g \sum_{g'} T_g^{(2)}(\tau) \otimes T_g^{(1)}(\tau) \otimes |Z(\tau)|^2 \quad (19a)$$

and

$$\xi = 2\pi\alpha/A^{1/2}. \quad (19b)$$

Equation (19) can be conveniently written as

$$I_D(\tau) = \xi^4 \{T^{(2)}(\tau) \otimes T^{(1)}(\tau) \otimes |Z(\tau)|^2\}, \quad (20)$$

where

$$T^{(n)} \equiv \sum_g T_g^{(n)}(\tau). \quad (21)$$

The calculation of the Z function can be performed with the multislice theory. Equation (20) is the general solution for double inelastic electron scattering. The incoherence of these states has been evaluated in (20). Electron diffraction from different 'frozen' lattice models in TDS, for example, can be covered with this single calculation. This is the unique advantage of this theory.

Equation (20) is derived based on an assumption of 'independent' scattering events. This has neglected the virtual inelastic corrections introduced by other processes (Yoshioka, 1957). It is important to note that an imaginary part should be introduced in the atomic potential V [(5b)] in order to take into account absorption effects.

3.2. *Double-phonon scattering*

Phonon scattering is generated by atomic vibrations in the crystal. The thermal vibration introduces a small time-dependent displacement to each atom, which gives a small correction to the potential of the equilibrium lattice. The first-order correction to the crystal potential due to atomic vibrations is (Takagi, 1958)

$$\Delta V(\mathbf{r}) = \sum_h \sum_l \{V_l[\mathbf{r}-\mathbf{R}(h)-\mathbf{r}(l)-\mathbf{u}(_l^h)] - V_l[\mathbf{r}-\mathbf{R}(h)-\mathbf{r}(l)]\} \quad (22)$$

where $V_l(\mathbf{r})$ is the lth atomic potential and $\mathbf{u}(_l^h)$ is the displacement of the lth atom in the hth unit cell which can be expressed as a sum of normal harmonic oscillator modes of momentum $\mathbf{q}$, frequency $\omega_j(\mathbf{q})$ and polarization vector $\mathbf{e}(l|_j^q)$ (Born, 1942; Brüesch, 1982):

$$\mathbf{u}(_l^h) = (\hbar/2Nm_l)^{1/2} \sum_q \sum_j [\omega_j(\mathbf{q})]^{-1/2} \mathbf{e}(l|_j^q) \times \exp\{i\mathbf{q}.[\mathbf{R}(h)+\mathbf{r}(l)]\}[a^+(_j^{-q}) + a(_j^q)], \quad (23)$$

where N is the total number of primitive unit cells in the crystal; m_l is the mass of the lth atom; a^+ and a are defined as the creation and annihilation operators of a phonon with momentum $\mathbf{q}$ and frequency $\omega_j(\mathbf{q})$, respectively, and j indicates different acoustic and optical branches. For a 3D periodic structure, using the relationship

$$\sum_h \exp[i\tau\mathbf{R}(h)] = [(2\pi)^3/V_c] \sum_g \delta(\tau-\mathbf{g}), \quad (24)$$

where $\mathbf{g}$ is a 3D reciprocal-lattice vector, the interaction Hamiltonian for creating a phonon of momentum $\mathbf{q}$ and frequency $\omega_j(\mathbf{q})$ is (Whelan, 1965a, b; Rez *et al.*, 1977)

$$H'(\mathbf{r}, \mathbf{q}, \omega) = \langle N(\mathbf{q}, \omega)+1|[-e\Delta V(\mathbf{r})]|N(\mathbf{q}, \omega)\rangle \simeq -ie(2\pi)^3 \sum_l \sum_g A_l[\omega_j(\mathbf{q})] \times \mathbf{e}(l|_j^q) \cdot (\mathbf{g}-\mathbf{q}) V_l(\mathbf{g}-\mathbf{q}) \times \exp[i(\mathbf{q}-\mathbf{g}).\mathbf{r}] \exp[i\mathbf{g}.\mathbf{r}(l)], \quad (25)$$

where

$$V_l(\mathbf{g}) = V_c^{-1} \int V_l(\mathbf{r}) \exp(-i\mathbf{g}.\mathbf{r}) \, d\mathbf{r}; \quad (26)$$

$N(\mathbf{q}, \omega)$ is the occupation number of the phonon state $|N(\mathbf{q}, \omega)\rangle$,

$$N(\mathbf{q}, \omega) = [\exp(\hbar\omega_j/k_BT)-1]^{-1} \quad (27a)$$

and

$$A_l(\omega_j(\mathbf{q})) \equiv \{\hbar(N(\mathbf{q}, \omega)+1)/2\omega_j(\mathbf{q})m_lN\}^{1/2} \quad (27b)$$

is the atomic vibration amplitude in phonon mode $\omega_j(\mathbf{q})$. Thus,

$$H_g'(\tau) = -ie(2\pi)^3 \sum_l A_l(\omega_j(\tau)) \, \mathbf{e}(l|_j^\tau) \cdot \tau \times V_l(\tau) \exp[i\mathbf{g}.\mathbf{r}(l)]. \quad (28)$$

Putting (28) in (18) and (21), summing over different phonon branches and defining

$$P_l(\tau) = a_3 e^2 N(2\pi)^5 \theta(\tau) \sum_j \int_{BZ} dq_z |A_l(\omega_j(\tau)) \times [\mathbf{e}(l|_j^\tau) \cdot \tau] V_l(\tau)|^2 \quad (29a)$$

as the phonon scattering function, where a 'switch' function is defined as

$$\theta(\tau) \equiv \begin{cases} 1 & \text{if } \tau \text{ falls within the first BZ} \\ 0 & \text{otherwise} \end{cases} \quad (29b)$$

and N is the total number of primitive unit cells in the crystal, one obtains

$$T^{(TDS)} = \sum_l P_l(\tau). \quad (30)$$

The relationship

$$\sum_g \exp\{i\mathbf{g}.[\mathbf{r}(l)-\mathbf{r}(l')]\} = N\delta_{ll'} \quad (31)$$

was used in deriving (30), where l and l′ are restricted

to the atoms in the same unit cell. According to (20), the intensity distribution in a double-TDS diffraction pattern is

$$I_{D-\mathrm{TDS}} = \xi^4 \left\{ \sum_{l_2} \sum_{l_1} P_{l_2}(\tau) \otimes P_{l_1}(\tau) \right\} \otimes \{|Z(\tau)|^2\}, \quad (32)$$

where the summations of l_1 and l_2 are restricted to the atoms in the same unit cell. The terms purely related by lattice dynamics are included in the first { } bracket. The terms related by dynamical electron scattering appear in the second { } bracket; these terms are determined solely by the elastic-scattering Schrödinger equation [(5*b*)] and can be solved using the multislice method (Cowley & Moodie, 1957). The scattering function of the double-phonon process is the convolution result of those for two single-inelastic-scattering processes. This convolution of the angular distribution function of a single-inelastic-scattering process with itself leads to a broader distribution. Equation (31) is consistent with the multiple diffuse scattering theory of Høier (1973). If one puts (27) into (29*a*), the TDS streaks observed in electron diffraction patterns are approximately determined by (Honjo, Kodera & Kitamura, 1964; Komatsu & Teramoto, 1966; Wang, 1991), $P_l(\tau) \simeq \sum_j [\omega_j(\tau)]^{-1}$, where $\omega_j(\mathbf{q})$ is the phonon dispersion relationship determined by the 2D atomic vibrations in the (*hkl*) plane perpendicular to the incident-beam direction $\mathbf{B} = [hkl]$. The TDS streaks are defined by the $\tau_x - \tau_y$ curves which satisfy $\omega_j(\tau) = 0$. The sharpness of the TDS streaks will be degraded by multiple-scattering effects because of the convolution of the P function which occurs in (31). This is in agreement with the experimental observations shown in Fig. 2. The TDS streaks can only be clearly resolved from the background scattering if the specimen is thin (Fig. 2*a*). In this case, only single inelastic scattering is important. Multiple scattering smears out the TDS streaks if the specimen is thick (Fig. 2*b*); the intensity distribution of the TDS electrons can be taken as a 'uniform' background.

3.3. *Double single-electron excitations*

Single-electron excitation is another inelastic scattering process in electron diffraction and is generated by exciting an atomic inner shell. Since this process is mainly determined by the properties of a single atom, it is thus possible to use the tight-binding approximation for calculating $H_g'^{(n)}$. Whelan (1965*a*) gave

$$H_g'^{nm} = (e^2/V_s\varepsilon_0)\varepsilon_{nm}(\mathbf{g}-\mathbf{q})/|\mathbf{g}-\mathbf{q}|^2, \quad (33a)$$

where

$$\varepsilon_{nm}(\mathbf{K}) = \langle n| \exp(-i\mathbf{K}\cdot\mathbf{r})|m\rangle, \quad (33b)$$

$|n\rangle$ and $|m\rangle$ are the normalized one-electron atomic wave functions and V_s is the volume of the crystal. If the contributions of all the atoms are considered, one obtains

$$H'_{nm}(\mathbf{r},\mathbf{q}) = (e^2/V_c\varepsilon_0) \sum_{\mathbf{g}} \sum_{\mathrm{I}} [\varepsilon^{\mathrm{I}}_{nm}(\mathbf{g}-\mathbf{q})/|\mathbf{g}-\mathbf{q}|^2] \times \exp[i(\mathbf{q}-\mathbf{g})\cdot\mathbf{r}] \exp[i\mathbf{g}\cdot\mathbf{r}(\mathrm{I})]. \quad (34)$$

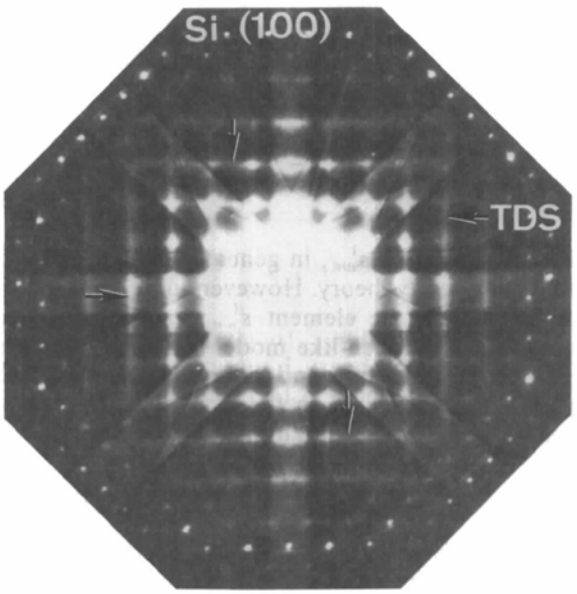

(*a*)

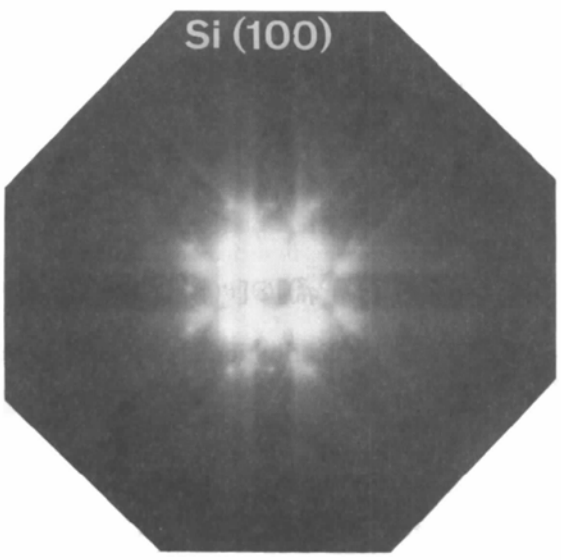

(*b*)

Fig. 2. Diffraction patterns from (*a*) a thin Si (001) crystal showing the TDS streaks along ⟨110⟩ and (*b*) the multiple-inelastic-scattering background from a thicker Si crystal. The visibility of the TDS streaks is degraded partially due to multiple-inelastic-scattering effects.

Comparison of (34) with (14*a*) gives

$$H_g^{l'nm}(\tau) = (e^2/V_c\varepsilon_0)\sum_l [\varepsilon_{nm}^l(\tau, q_0)/\tau^2 + q_0^2] \times \exp[i\mathbf{g}\cdot\mathbf{r}(l)], \quad (35a)$$

where

$$q_0 \simeq k_0(E - E_1)/2E. \quad (35b)$$

Using (31), one obtains

$$T^{(S)} = [e^2/V_c\varepsilon_0]^2 N\theta(\tau)\sum_l [|\varepsilon_{10}^l(\tau, q_0)|^2/(\tau^2 + q_0^2)^2]. \quad (36)$$

The calculation of ε_{nm}^l, in general, involves complicated many-body theory. However, under reasonable approximation, the element ε_{nm}^l can be calculated based on a hydrogen-like model for some light elements, such as carbon and silicon (Egerton, 1986). In (35), ε_{nm}^l is related to the generalized oscillator strength (GOS) f_{nm}^l (Inokuti, 1971) by

$$f_{nm}^l = (|E_n - E_m|/\Re a_0^2)|\varepsilon_{nm}^l|^2/(\tau^2 + q_0^2), \quad (37)$$

where $\Re = 13{\cdot}6$ eV is the Rydberg energy and $a_0 = 0{\cdot}053$ nm is the Bohr radius. Since f_{nm}^l depends weakly on τ, one can approximately take f_{nm}^l out of the convolution operation. For double single-electron excitations, using (20) and (37), the intensity distribution in the double single-electron scattered diffraction pattern is

$$I_{D-S} \simeq \xi^4[e^2/V_c\varepsilon_0]^4[N^2(\Re a_0^2)^2/(E - E_1)(E - E_2)] \times \left\{\sum_{l_2}\sum_{l_1} |f_{10}^{l_1} f_{20}^{l_2}|\right\}\{C(\tau)\otimes|Z(\tau)|^2\}, \quad (38)$$

where

$$C(\tau) \simeq [\theta(\tau)/(\tau^2 + q_0^2)]\otimes[\theta(\tau)/(\tau^2 + q_0^2)]. \quad (39)$$

The electron angular distribution is contained in the last { } bracket.

3.4. *Phonon–single-electron excitations*

If one puts (30), (36) and (37) into (20), the diffraction pattern formed by phonon–single-electron excitations is

$$I_{D-S} \simeq \xi^4[e^2/V_c\varepsilon_0]^2[\Re a_0^2/(E - E_2)]\sum_{l_2}\sum_{l_1} |f_{20}^{l_2}|P_{l_1}(\tau) \otimes[\theta(\tau)/(\tau^2 + q_0^2)]\otimes|Z(\tau)|^2. \quad (40)$$

3.5. *Valence excitations*

Valence (or plasmon) losses are generated by the collective excitations of the electrons in the crystal. These processes usually involve small energy loss (about 10–30 eV) and small momentum transfers. Valence excitations are characterized by the dielectric response function $\varepsilon(\omega, \mathbf{q})$ of the system. According to the result of Okamoto *et al.* (1971), the scattering function for valence excitation can be written as

$$T_g^{(V)} = [e^2\hbar V_s/\pi\varepsilon_0]\theta(\tau)\int_0^\infty d\omega \times \mathrm{Im}\{-[\varepsilon(\tau, -\tau - g, \omega)]^{-1}\}[\tau^2 + (\omega/v)^2]^{-1}, \quad (41)$$

where ε is the generalized energy-loss function and ω is frequency. If only the $g = 0$ term is important, so that $\varepsilon(\tau, -\tau - \mathbf{g}, \omega)$ becomes the usual dielectric function $\varepsilon(\tau, \omega)$, one has

$$T^{(V)} \simeq T_0^{(V)} = [e^2\hbar V_s/\pi\varepsilon_0]\theta(\tau) \times \int_0^\infty d\omega\ \mathrm{Im}\{-[\varepsilon(\tau, \omega)]^{-1}\} \times [\tau^2 + (\omega/v)^2]^{-1}. \quad (42)$$

Therefore, the diffraction patterns for valence-phonon, valence-single-electron and valence-valence double excitations can be obtained by using the corresponding $T^{(V)}$ [(42)], $T^{(\mathrm{TDS})}$ [(30)] and $T^{(S)}$ [(36)] in (20), respectively. The lengthy results will not be listed here.

It is important to note that the phase shift in inelastic scattering has been evaluated in (31) before any numerical calculation. The calculations of T functions depend only on the modulus squared of the scattering-matrix element. This is a key point which makes this theory more powerful than any other theories. The T functions for phonon and valence excitations can be directly calculated if the phonon dispersion relationships and medium dielectric functions are known, respectively.

4. Multiple-scattering theory

Before proposing the multiple-scattering theory, one considers a triple-scattering process (ϕ_T). The crystal can be considered as either in its ground state (elastic) or in one of its three 'independent' excited states. The transitions from the ground state to each of the three states can be described separately by (8). An electron can be scattered in 3! difference sequences among the three inelastic states (see Fig. 1*b*). Using the double scattering result in (9) and through (7*a*), one obtains

for triple inelastic scattering

$$\partial\phi_T(\mathbf{r})/\partial z = \alpha^3\Big\{ U_{(3)}(\mathbf{r}) \int_0^z \mathrm{d}z_2\, U_{(2)}(\mathbf{b}, z_2) \times \int_0^z \mathrm{d}z_1\, U_{(1)}(\mathbf{b}, z_1) + U_{(2)}(\mathbf{r}) \int_0^z \mathrm{d}z_2 U_{(1)}(\mathbf{b}, z_2) \times \int_0^z \mathrm{d}z_1\, U_{(3)}(\mathbf{b}, z_1) + U_{(1)}(\mathbf{r}) \int_0^z \mathrm{d}z_2\, U_{(2)}(\mathbf{b}, z_2) \times \int_0^z \mathrm{d}z_1\, U_{(3)}(\mathbf{b}, z_1)\Big\}. \quad (43)$$

The solution of (43) is

$$\phi_T(\mathbf{r}) = \alpha^2\Big\{ \int_0^z \mathrm{d}z_3\, U_{(3)}(\mathbf{b}, z_3) \int_0^z \mathrm{d}z_2\, U_{(2)}(\mathbf{b}, z_2) \times \int_0^z \mathrm{d}z_1\, U_{(1)}(\mathbf{b}, z_1)\Big\}. \quad (44)$$

It can be generalized from (10) and (44) that the electron wave function after being multiply inelasti10cally scattered for m times among the m states is

$$\phi_m(\mathbf{r}) = c_0\alpha^m \prod_{n=1}^{m} \int_0^z \mathrm{d}z_n U_{(n)}(\mathbf{b}, z_n) \quad \text{for } m \geq 1; \quad (45a)$$

$$\phi_0(\mathbf{r}) = c_0. \quad (45b)$$

It can be proved directly from (45a) that

$$\partial\phi_m(\mathbf{r})/\partial z = \alpha \sum_{n=1}^{m} U_{(n)}\phi_{m'}(\mathbf{r})|_{m'=m-1\neq n}, \quad (46)$$

where $\phi_{m'}(\mathbf{r})|_{m'=m-1\neq n}$ means the m'th-order multiple inelastic scattering among the $(m-1)$ events excluding event n and is determined by (45a). Equation (46) is equivalent to (7a) if the approximations addressed at the beginning of § 3.1 are considered. A constant c_0 is introduced in (45) to take into account the absorption effect in order to normalize the total scattering intensity. Following the analogous procedures as used from (10) to (20), the intensity distribution contributed by the mth multiple inelastic scattering is

$$I_m(\tau) = (c_0\xi^m)^2\{T^{(m)}(\tau)\otimes T^{(m-1)}(\tau)\otimes\ldots\otimes T^{(1)}(\tau)\} \otimes|Z_m(\tau)|^2, \quad (47a)$$

where

$$Z_m(\tau) \equiv S_{(m)}(\tau)\otimes S_{(m-1)}(\tau)\otimes\ldots\otimes S_{(1)}(\tau) \otimes \Psi_0^0(\tau, d), \quad (47b)$$

$$S_{(m)}(\tau) = \int_0^d \mathrm{d}z \exp[iq_{(m)}z]S_{(m)}(\tau, z) \quad (48a)$$

and

$$q_{(m)} = k_m(E - E_m)/2E. \quad (48b)$$

The physical meaning of (46) and (47) can be understood as follows. The effects of multiple scattering are equivalent partially to broadening the single-scattering function $[T^{(n)}]$ by those of other processes and partially to rescattering the Kikuchi patterns ($|S_{(1)}\otimes\Psi_0^0|^2$) produced in one single-scattering process by others. The convolution operations of $S_{(n)}$ functions in (47) mean the convolutions of Kikuchi patterns produced by different inelastic-scattering processes. The commutative property of the convolution operations in (47a) shows that there will be no difference whichever process is considered first in the calculations. Also, (47) can be applied to the single-scattering case simply by taking $m = 1$.

5. Contributions of TDS electrons to high-angle annular-dark-field images in STEM

The high-angle annular-dark-field (ADF) STEM image is formed by collecting the large-angle-scattered electrons when a small electron probe scans across a specimen (Pennycook & Boatner, 1988; Xu, Kirkland, Silcox & Keyse, 1990). It has been shown that TDS takes the dominant role in determining image contrast based on a single-phonon-scattering model (Wang & Cowley, 1990). Now one considers the contributions of multiple phonon scattering. If an incident electron probe $\Psi_0^0(\mathbf{b}, d) = \Psi_0^0(\mathbf{b}-\mathbf{b}_0, d)$ is centred at $\mathbf{b}_0$, the contribution from double phonon scattering can be derived as follows. Putting (22) and (23) in (25), one obtains

$$H'(\mathbf{r}, \mathbf{q}, \omega) \simeq -e\sum_h\sum_l A_l[\omega_j(\mathbf{q})]\mathbf{e}(l|_j^q)\cdot\nabla V_l[\mathbf{r}-\mathbf{R}(h)-\mathbf{r}(l)] \times\exp\{i\mathbf{q}\cdot[\mathbf{R}(h)+\mathbf{r}(l)]\}. \quad (49)$$

Equation (49) is the result of the single-phonon-excitation model. The small-angle approximation was not introduced when deriving (49). Using (13) and assuming that all the phonon-scattered electrons have been collected by the ADF detector, the contribution of the electrons in phonon mode $(\mathbf{q}, \omega)$ to the ADF

STEM image is

$$\int_{-\infty}^{\infty} d\tau |\Psi_D(\tau, d)|^2 = \int_{-\infty}^{\infty} d\mathbf{b}\, |\Psi_D(\mathbf{b}, d)|^2 = \alpha^4 \int d\mathbf{b} \left\{ \left| \int_0^d dz_1 H'_{(1)}(\mathbf{b}, z_1, \mathbf{q}) S_{(1)}(\mathbf{b}-\mathbf{b}_0, z_1) \right|^2 \times \left| \int_0^d dz'_1\, H'_{(2)}(\mathbf{b}, z'_1, \mathbf{q}') S_{(2)}(\mathbf{b}-\mathbf{b}_0, z'_1) \right|^2 \times |\Psi_0^0(\mathbf{b}-\mathbf{b}_0, d)|^2 \right\}. \quad (50)$$

Now if the crystal is cut into many slices of equal thickness Δz, the integration of z_1 can be written as a sum of n slices,

$$\int d\tau |\Psi_D(\tau, d)|^2 \simeq \alpha^4 (\Delta z)^4 \int d\mathbf{b} \left\{ \left| \sum_n H'_{(1)}(\mathbf{b}, z_n, \mathbf{q}) S_{(1)}(\mathbf{b}-\mathbf{b}_0, z_n) \right|^2 \times \left| \sum_{n'} H'_{(2)}(\mathbf{b}, z'_n, \mathbf{q}') S_{(2)}(\mathbf{b}-\mathbf{b}_0, z'_n) \right|^2 \times |\Psi_0^0(\mathbf{b}-\mathbf{b}_0, d|^2 \right\}. \quad (51)$$

Since H' is a peak function at each atomic site for localized inelastic scattering, the square of the sum can be approximately given by a sum of the squares and one obtains

$$\int d\tau |\Psi_D(\tau, d)|^2 \simeq \alpha^4 (\Delta z)^4 \int d\mathbf{b} \left\{ \left[\sum_n |H'_{(1)}(\mathbf{b}, z_n, \mathbf{q}) S_{(1)}(\mathbf{b}-\mathbf{b}_0, z_n)|^2 \right] \times \left[\sum_{n'} |H'_{(2)}(\mathbf{b}, z_{n'}, \mathbf{q}') S_{(2)}(\mathbf{b}-\mathbf{b}_0, z_{n'})|^2 \right] \times |\Psi_0^0(\mathbf{b}-\mathbf{b}_0, d)|^2 \right\}. \quad (52)$$

Summing (52) for different phonon branches j and j' and phonon modes $\mathbf{q}$ and $\mathbf{q}'$, the image intensity contributed by double-phonon processes at $\mathbf{b}_0$ is

$$I_{(2)}(\mathbf{b}_0) = [V_c/(2\pi)^3]^2 \sum_{j=1} \int_{BZ} d\mathbf{q} \sum_{j'=1} \int_{BZ} d\mathbf{q} \times \int d\tau |\Psi_D(\tau, d)|^2 = \alpha^4 (\Delta z)^4 \int d\mathbf{b} \left\{ \left[\sum_n [V_c/(2\pi)^3] \times \sum_{j=1} \int_{BZ} d\mathbf{q} |H'(\mathbf{b}, z_n, \mathbf{q}) S(\mathbf{b}-\mathbf{b}_0, z_n)|^2 \right]^2 \times |\Psi_0^0(\mathbf{b}-\mathbf{b}_0, d)|^2 \right\}. \quad (53)$$

Putting (25) into (53), assuming that V_l is a sharp peak function located on atomic nuclei and neglecting the $\mathbf{q}$ and ω dependence of $\mathbf{e}$, one obtains

$$I_{(2)}(\mathbf{b}_0) \simeq \int d\mathbf{b} \left[\sum_n G^2(\mathbf{b}, z_n) |S(\mathbf{b}-\mathbf{b}_0, z_n)|^2 \right]^2 \times |\Psi_0^0(\mathbf{b}-\mathbf{b}_0, d)|^2, \quad (54)$$

where the TDS generation function of the nth slice is

$$G^2(\mathbf{b}, z_n) = (e\alpha)^2 \sum_n \sum_l \overline{A_l^2} \times (\{\partial v_l[\mathbf{b}-\mathbf{R}_b(h)-\mathbf{r}_b(l)]/\partial x\}^2 + \{\partial v_l[\mathbf{b}-\mathbf{R}_b(h)-\mathbf{r}_b(l)]/\partial y\}^2), \quad (55)$$

where the summations over h and l are restricted to the atoms falling in the nth slice; the average amplitude square is defined as

$$\overline{A_l^2} = [V_c/(2\pi)^3] \sum_{j=1} \int_{BZ} d\mathbf{q}\, A_l^2[\omega_j(\mathbf{q})] \quad (56)$$

and v_l is the projected atomic potential in the xy plane,

$$v_l[\mathbf{b}-\mathbf{R}_b(h)-\mathbf{r}_b(1)] = \int_{z_n}^{z_n+\Delta z} dz\, V_l[\mathbf{b}-\mathbf{R}_b(h)-\mathbf{r}_b(l), z]. \quad (57)$$

Equation (54) is not limited by the assumption of 3D periodic structure; defects or imperfections can be included in the calculations by generalizing (55) as

$$G^2(\mathbf{b}, z_n) = (e\alpha)^2 \sum_i \overline{A_i^2} (\{\partial v_i[\mathbf{b}-\mathbf{r}_b(i)]/\partial x\}^2 + \{\partial v_i[\mathbf{b}-\mathbf{r}_b(i)]/\partial y\}^2), \quad (58)$$

where the sum over i is over all the atoms falling in the nth slice. It is necessary to point out that (54) was derived by neglecting the $\mathbf{q}$ dependence of the S function defined in (11b), which means that the 'inclined incidence' effect (or $\mathbf{q}$ correction to wave vector $\mathbf{k}$) of phonon scattering is neglected (Wang, 1991).

Similar procedures can be applied to consider higher-order effects. For the mth order of multiple phonon scattering, one can obtain

$$I_{(m)}(\mathbf{b}_0) = f_n \int d\mathbf{b} \left[\sum_n G^2(\mathbf{b}, z_n) |S(\mathbf{b}-\mathbf{b}_0, z_n)|^2 \right]^m \times |\Psi_0^0(\mathbf{b}-\mathbf{b}_0, d)|^2, \quad (59)$$

where a constant coefficient f_m is introduced for the normalization of total scattered intensity. If the multiple phonon scattering is governed by a Poisson distribution law, *i.e.*

$$f_m = f_0/m!, \quad (60)$$

the total contribution of phonon scattering to the

ADF STEM image is

$$I_{\mathrm{TDS}}(\mathbf{b}_0) = \sum_{m=1}^{\infty} I_{(m)}(\mathbf{b}_0) = f_0 \int \mathrm{d}\mathbf{b} \left\{ \exp\left[\sum_n G^2(\mathbf{b}, z_n) |S(\mathbf{b}-\mathbf{b}_0, z_n)|^2 \right] - 1 \right\} \times |\Psi_0^0(\mathbf{b}-\mathbf{b}_0, d)|^2. \quad (61)$$

Equations (59) and (61) were derived based on an assumption that the ADF detector is so large that all the phonon-scattered electrons have been collected by the ADF detector. In practice, a finite detection function $D(\tau)$ can be introduced in calculations by replacing the atomic scattering factor by

$$V_{\mathrm{i}}'(\tau) = D(\tau) V_{\mathrm{i}}(\tau), \quad (62)$$

which means that the Fourier components falling outside the ADF detector angular range can be dropped off in the atomic scattering factor (Wang & Cowley, 1990). It is worth noting that (61) cannot be written in a convolution form.

Now consider the validity of the single-phonon-scattering model. The contribution of single-phonon excitation to the ADF image is given by

$$I_{(1)}(\mathbf{b}_0) = f_0 \int \mathrm{d}\mathbf{b} \left\{ \sum_n G(\mathbf{b}, z_n) |S(\mathbf{b}-\mathbf{b}_0, z_n)|^2 \right\} \times |\Psi_0^0(\mathbf{b}-\mathbf{b}_0, d)|^2. \quad (63)$$

Thus, single scattering [(63)] approximates multiple scattering [(61)] if

$$\left\{ \sum_n G^2(\mathbf{b}, z_n) |S(\mathbf{b}-\mathbf{b}_0, z_n)|^2 \right\} \ll 1. \quad (64)$$

However, this condition may not be satisfied when $\mathbf{b}$ is close to the equilibrium positions of atomic nuclei. Consider the following simple model. If an atomic potential can be represented by a Gaussian function,

$$v_1 \simeq v_0 \exp(-b^2/r_0^2), \quad (65)$$

where v_0 and r_0 are the depth and radius of the atomic potential well, respectively, and S is approximately of the order $1/k_0 = \lambda/2\pi$ (see Appendix *B*), the maximum value of $\{\sum_n G^2|S|^2\}$ can be evaluated as

$$\left\{ \sum_n G^2|S|^2 \right\}_{\max} \simeq \pi^2 (v_0/V_0)^2 (A_1/r_0)^2 (\Delta z/\lambda)^2 N_0, \quad (66)$$

where N_0 is the total number of crystal slices. Typically, if $v_0 \simeq 1$ kV, $V_0 \simeq 100$ kV, $A_1 \simeq 0{\cdot}01$ nm, $r_0 \simeq 0{\cdot}05$ nm, $\Delta z \simeq 0{\cdot}2$ nm, $\lambda \simeq 0{\cdot}0037$ nm and $N_0 = 50$, (66) yields

$$\left\{ \sum_n G^2|S|^2 \right\}_{\max} \simeq 6. \quad (67)$$

Therefore, condition (64) is not satisfied at the points close to the atomic nuclei. In practice, if the size of the electron probe is considerably larger than the atom size, the single-phonon-scattering model is a good approximation. Multiple-scattering theory [(61)] may be necessary for quantitative image analysis. It is interesting to note that the 'target' scattering function of the multiple-phonon model [*i.e.* the term in the square brackets in (59)] is sharper than that of the single-phonon model [*i.e.* the term in the curly brackets in (63)]. Therefore, the ADF STEM image formed by the multiple-phonon-scattered electrons may have higher resolution than that produced by the electrons after single-phonon scattering. This statement applies only to specimens with thickness less than about 10 nm.

6. Concluding remarks

A dynamical multiple elastic and inelastic electron scattering theory is proposed for 'independent' inelastic scattering events. By independent one means that the excitation of each state is not affected by the other states and can be treated separately using single inelastic scattering theory. In practice, the absorption effects introduced by different inelastic scattering processes can be included in the calculations of these 'independent' states. The plural scattering of phonon, single-electron and valence (or plasmon) excitations can be comprehensively included in a single formula. The scattering functions for these different types of inelastic scattering events have been derived and applied to double inelastic processes. The most important advantage of this new theory is that the incoherence of all the possible inelastic scattering processes of different energies and momenta can be evaluated analytically before any numerical calculations, providing an easy way of evaluating coherence, incoherence and partial coherence in electron diffraction calculations. The quasi-elastic scattering of electrons from crystal lattices of different 'frozen' configurations in thermal diffuse scattering (TDS) (in terms of semiclassical theory), for example, can be covered in just a single calculation.

The effects of multiple scattering are equivalent partially to the broadening of the scattering function of a single inelastic process by those of others and partially to the rescattering of the Kikuchi pattern produced in one scattering process by others. The final diffraction pattern is a convoluted result of those Kikuchi patterns produced by different inelastic-scattering processes.

In this new theory, only the modulus squared of the scattering-matrix element is needed; the phase shift of inelastic scattering has been evaluated before any numerical calculation. Compared with the Bloch-wave theory (see Maslen & Rossouw, 1984), this is an important advantage of the new theory. In

addition, the equivalence of this theory with the inelastic multislice theory has been proved.

Finally, the theory of multiple-phonon excitations in simulating high-angle annular-dark-field (ADF) scanning transmission electron microscopy (STEM) images is proposed. It is shown that the single-phonon-scattering model is a good approximation except at points close to atomic nuclei if the electron probe is comparable in size to that of an atom. It is suggested that higher-order phonon scattering may improve the resolution of the ADF STEM images.

The author is grateful to Drs J. Bentley and K. B. Alexander for many discussions and to the referees for useful suggestions. This research was sponsored by the Division of Materials Sciences, US Department of Energy, under contract DE-AC05-84OR21400 with Martin Marietta Energy Systems, Inc.

APPENDIX *A*

Equivalence of (8*c*) with the inelastic multislice theory

For easy notation, one separates the wave function from its plane-wave part by defining

$$\Psi_n(\mathbf{r}) = \varphi_n(\mathbf{b}, z)\exp(i\mathbf{k}_n \cdot \mathbf{r}), \qquad (A.1a)$$

$$\Psi_n^0(\mathbf{r}) = \varphi_n^0(\mathbf{b}, z)\exp(i\mathbf{k}_n \cdot \mathbf{r}). \qquad (A.1b)$$

For the nth excited state, (8c) can be rewritten as

$$\varphi_n(\mathbf{b}, z) = a\int_0^z \mathrm{d}z' \{H'_{00}(\mathbf{b}, z')\Psi_0^0(\mathbf{b}, z') \times [\partial\Psi_n^0(\mathbf{b}, z')/\partial z]^{-1}\}\varphi_n^0(\mathbf{b}, z). \qquad (A.2)$$

By neglecting the back-scattering term under the small-angle approximation, in the multislice method, the solution of the elastic Schrödinger equation can be written (Cowley & Moodie, 1957; Ishizuka & Uyeda, 1977) as

$$\varphi_n^0(\mathbf{b}, z+\Delta z) = [\varphi_n^0(\mathbf{b}, z)Q(\mathbf{b}, z)] \otimes P_n(\mathbf{b}), \qquad (A.3)$$

where Q is the phase-grating function of the crystal slice Δz:

$$Q(\mathbf{b}, z) = \exp\left[i\sigma\int_z^{z+\Delta z} \mathrm{d}z'\, V(\mathbf{b}, z')\right]; \qquad (A.4)$$

the wave propagation function is

$$P_n(\mathbf{b}) = (i\Delta z\lambda_n)^{-1}\exp[i\pi b^2/2\lambda_n\Delta z]; \qquad (A.5)$$

$\sigma = e/\hbar v_0$; v_0 is the electron velocity; λ_n is the electron wavelength of energy E_n.

Now one derives the relationship which governs the inelastic wave $\varphi_n(\mathbf{b}, z)$ before and after being scattered by a very thin crystal slice of thickness Δz. From (*A*.2), one can directly write

$$\begin{aligned}
&\varphi_n(\mathbf{b}, z+\Delta z) - \varphi_n(\mathbf{b}, z) \\
&\quad = \alpha\int_0^z \mathrm{d}z' \{H'_{n0}(\mathbf{b}, z')\Psi_0^0(\mathbf{b}, z') \\
&\qquad \times [\partial\Psi_n^0(\mathbf{b}, z')/\partial z]^{-1}\} \\
&\qquad \times [\varphi_n^0(\mathbf{b}, z+\Delta z) - \varphi_n^0(\mathbf{b}, z)] \\
&\qquad + \alpha\int_z^{z+\Delta z} \mathrm{d}z' \{H'_{n0}(\mathbf{b}, z') \\
&\qquad \times \Psi_0^0(\mathbf{b}, z')[\partial\Psi_n^0(\mathbf{b}, z')\partial z]^{-1}\}\varphi_n^0(\mathbf{b}, z+\Delta z) \\
&\quad \simeq \varphi_n(\mathbf{b}, z)[\varphi_n^0(\mathbf{b}, z+\Delta z)/\varphi_n^0(\mathbf{b}, z) - 1] \\
&\qquad + \alpha\{h'_{n0}(\mathbf{b}, z)\Psi_0^0(\mathbf{b}, z)[\partial\Psi_n^0(\mathbf{b}, z)/\partial z]^{-1}\} \\
&\qquad \times \varphi_n^0(\mathbf{b}, z+\Delta z), \qquad (A.6)
\end{aligned}$$

where

$$h'_{n0} = \int_z^{z+\Delta z} H'_{n0}(\mathbf{b}, z')\,\mathrm{d}z'. \qquad (A.7)$$

Equation (*A*.6) can be conveniently written as

$$\begin{aligned}
\varphi_n(\mathbf{b}, z+\Delta z) &\simeq \varphi_n(\mathbf{b}, z)[\varphi_n^0(\mathbf{b}, z+\Delta z)/\varphi_n^0(\mathbf{b}, z)] \\
&\quad + \alpha\{h'_{n0}(\mathbf{b}, z)\Psi_0^0(\mathbf{b}, z) \\
&\quad \times [\partial\Psi_n^0(\mathbf{b}, z)/\partial z]^{-1}\}\varphi_n^0(\mathbf{b}, z+\Delta z). \qquad (A.8)
\end{aligned}$$

For fast electrons, it is always a good approximation to assume forward scattering (see Appendix *B*), so that

$$\begin{aligned}
\partial\Psi_n^0(\mathbf{b}, z)/\partial z &= [ik_{nz}\varphi_n^0(\mathbf{b}, z) + \partial\varphi_n^0(\mathbf{b}, z)/\partial z] \\
&\quad \times \exp(i\mathbf{k}_n \cdot \mathbf{r}) \\
&\simeq ik_{nz}\varphi_n^0(\mathbf{b}, z)\exp(i\mathbf{k}_n \cdot \mathbf{r}). \qquad (A.9)
\end{aligned}$$

With (*A*.9), (*A*.8) becomes

$$\begin{aligned}
\varphi_n(\mathbf{b}, z+\Delta z) &\simeq [\varphi_n(\mathbf{b}, z) - i\sigma h'_{n0}(\mathbf{b}, z)\varphi_0^0(\mathbf{b}, z)] \\
&\quad \times \{\varphi_n^0(\mathbf{b}, z+\Delta z)/\varphi_n^0(\mathbf{b}, z)\}. \qquad (A.10)
\end{aligned}$$

The physical meaning of (*A*.10) can be interpreted as follows. The first term in [...] [$\varphi_n(\mathbf{b}, z)$] is the inelastic wave generated before the wave arrives at the slice entrance face located at $z = z$. In the single-inelastic-scattering model, this part of the wave will only be elastically scattered when it penetrates the crystal slice and is responsible for the formation of Kikuchi patterns. The second term in [...] ($\sigma h'_{n0}\varphi_0^0$) is the newly generated inelastic wave when the elastic wave (φ_0^0) penetrates through the slice. The elastic scattering of these two parts within the slice is included in the term $\varphi_n^0(\mathbf{b}, z+\Delta z)/\varphi_n^0(\mathbf{b}, z)$. For a very thin slice ($\Delta z \to 0$), P_n is very close to a Dirac δ function, with (*A*.3), (*A*.10) can thus be

approximately written as

$$\varphi_n(\mathbf{b}, z+\Delta z) = [\varphi_n(\mathbf{b}, z) - i\sigma h'_{n0}(\mathbf{b}, z)\varphi_0^0(\mathbf{b}, z)] \times [\varphi_n^0(\mathbf{b}, z)Q(\mathbf{b}, z)] \otimes P_n/\varphi_n^0(\mathbf{b}, z) \simeq [Q(\mathbf{b}, z)\{\varphi_n(\mathbf{b}, z) - i\sigma h'_{n0}(\mathbf{b}, z)\varphi_0^0(\mathbf{b}, z)\}]P_n(\mathbf{b}). \quad (A.11)$$

Equation (*A*.11) is the exact form of the multislice theory for single inelastic scattering (Wang, 1989). This establishes the equivalence of (8*c*) with the other inelastic-scattering theories.

APPENDIX *B*

Calculations of $S_{(n)}$ and Z functions in the multislice scheme

For convenient notation, the subscript n in (5*b*) is dropped and $U = H'_{nn}(\mathbf{r})$. Equation (5*b*) can be written as

$$(\nabla^2 + k^2)\Psi^0 = (2m_e/\hbar^2)U(\mathbf{r})\Psi^0. \quad (B.1)$$

This equation is the standard elastic-scattering equation of high-energy electrons. By writing

$$\Psi^0 \equiv \varphi^0 \exp(i\mathbf{k}\cdot\mathbf{r}), \quad (B.2)$$

the calculation of φ^0 is governed by (*A*.3). In the multislice approach, a crystal is cut into many slices in the z direction and the atomic structure in each slice is projected onto a plane perpendicular to the z axis. It is not straightforward to find $\partial\Psi_n^0(\mathbf{r})/\partial z$ directly from Ψ_n^0 in the multislice approach. For this reason one starts from (*B*.1). If one puts (*B*.2) into (*B*.1) and neglects the $\partial^2\varphi^0/\partial z^2$ term, (*B*.1) becomes

$$\frac{\partial\varphi^0(\mathbf{r})}{\partial z} = \{(2m_e/\hbar^2)U(\mathbf{r})\varphi^0 - (\partial^2/\partial x^2 + \partial^2/\partial y^2)\varphi^0 - i2(k_x\,\partial/\partial x + k_y\,\partial/\partial y)\varphi^0\}/i2k_z. \quad (B.3)$$

Reintroduction of the n and m notation gives

$$S_{(m)}(\mathbf{r}) \equiv \frac{\Psi_0^0(\mathbf{r})}{\partial\Psi_m^0(\mathbf{r})/\partial z} = \frac{\varphi_0^0 \exp[i(\mathbf{k}_0 - \mathbf{k}_m)\cdot\mathbf{r}]}{ik_{mz}\varphi_m^0 + \partial\varphi_m^0(\mathbf{r})/\partial z} = \varphi_0^0 \exp[i(\mathbf{k}_0 - \mathbf{k}_m)\cdot\mathbf{r}] \times \{ik_{mz}\varphi_m^0 + [-(2m_e e/\hbar^2)V(\mathbf{r})\varphi_m^0 - (\partial^2/\partial x^2 + \partial^2\partial y^2)\varphi_m^0 - i2(k_{mx}\,\partial/\partial x + k_{my}\,\partial/\partial y)\varphi_m^0]/i2k_{mz}\}^{-1}, \quad (B.4)$$

where the calculation of φ_0^0 and φ_m^0 is governed by (*A*.3). The momentum transfer during the inelastic transition from the mth state to the nth state is $\mathbf{q}_{mn} = \mathbf{k}_n - \mathbf{k}_m$. In (*B*.4), crystal potential V and the Laplace operator characterize the elastic rescattering of the inelastic wave. Therefore, the $S_{(m)}$ function is responsible for the formation of Kikuchi lines. For high-energy electrons, to a good approximation, the first term in the denominator of (*B*.4) is much larger than the remaining terms; thus

$$S_{(m)}(\mathbf{r}) \simeq \varphi_0^0 \exp(i\mathbf{q}_{m0}\cdot\mathbf{r})/ik_{mz}\varphi_m^0. \quad (B.5)$$

If $\varphi_0^0 \simeq \varphi_m^0$, $|S_{(m)}| \simeq 1/k_{mz}$.

Note added in proof: Recent numerical calculations have found that the $S_{(n)}(\mathbf{b}, z)$ function defined in (11*b*) is very important in the formation of Kikuchi patterns. In this paper, the momentum transfer involved in a single-inelastic-scattering process is approximately represented by an average value $\mathbf{q}_n$ when deriving (20) and (47). In practical calculations, the $S_{(n)}$ function take the form

$$S_{(n)}(\mathbf{r}) \equiv \Psi_0^0(\mathbf{r}, E_0)[\partial\Psi_0^0(\mathbf{r}, E_n, \mathbf{q}_n)/\partial z]^{-1},$$

where $\Psi_0^0(\mathbf{r}, E_0)$ and $\Psi_0^0(\mathbf{r}, E_n, \mathbf{q}_n)$ are the multislice solutions of (5*b*) for electrons of incident energies E_0 and E_n and wave vectors $\mathbf{k}$ and $\mathbf{k}+\mathbf{q}_n$, respectively. The selection of $\mathbf{q}_n$ can critically affect the appearance of the final Kikuchi pattern (Wang, in preparation).

References

BIRD, D. M. & WRIGHT, A. G. (1989). *Acta Cryst.* A**45**, 104-109.

BORN, M. (1942). *Rep. Prog. Phys.* **9**, 294-333.

BRÜESCH, P. (1982). *Phonons: Theory and Experiments* I - *Lattice Dynamics and Models of Interatomic Forces.* Berlin, Heidelberg, New York: Springer-Verlag.

COWLEY, J. M. & MOODIE, A. F. (1957). *Acta Cryst.* **10**, 609-619.

COWLEY, J. M. & POGANY, A. P. (1968). *Acta Cryst.* A**24**, 109-116.

DOYLE, P. A. (1969). *Acta Cryst.* A**25**, 569-577.

DUDAREV, S. L. & RYAZANOV, M. I. (1988). *Acta Cryst.* A**44**, 51-61.

EGERTON, R. F. (1986). *Electron Energy-Loss Spectroscopy in Electron Microscope.* New York: Plenum Press.

FANIDIS, C., VAN DYCK, D., COENE, W. & VAN LANDUYT, J. (1989). *Computer Simulation of Electron Microscope Diffraction and Images*, edited by W. KRAKOW & M. O'KEEFE, pp. 135-137. London: The Minerals, Metals and Materials Society.

FANIDIS, C., VAN DYCK, D. & VAN LANDUYT, J. (1990). *Proc. XII Int. Congr. for Electron Microscopy, Seattle*, Vol. 1, edited by L. D. PEACHEY & D. B. WILLIAMS, pp. 58-59. San Francisco Press.

GJØNNES, J. (1966). *Acta Cryst.* **20**, 240-249.

GJØNNES, J. & WATANABE, D. (1966). *Acta Cryst.* **21**, 297-302.

HALL, C. R. (1965). *Philos. Mag.* **12**, 815-826.

HALL, C. R. & HIRSCH, P. B. (1965). *Proc. R. Soc. London Ser. A*, **286**, 158-177.

HØIER, R. (1973). *Acta Cryst.* A**29**, 663-672.

HONJO, G., KODERA, S. & KITAMURA, N. (1964). *J. Phys. Soc. Jpn*, **19**, 351-367.

HOWIE, A. (1963). *Proc. R. Soc. London*, **271**, 268-287.

HUMPHREYS, C. J. & WHELAN, M. J. (1969). *Philos. Mag.* **20**, 165-172.

INOKUTI, M. (1971). *Rev. Mod. Phys.* **43**, 297-347.

ISHIZUKA, K. & UYEDA, N. (1977). *Acta Cryst.* A**33**, 740-749.

KOMATSU, K. & TERAMOTO, K. (1966). *J. Phys. Soc. Jpn*, **21**, 1152-1159.

LOANE, R. F., XU, P. & SILCOX, J. (1991). *Acta Cryst.* A**47**, 267-273.

MASLEN, V. W. & ROSSOUW, C. J. (1984). *Philos. Mag.* **49**, 735-757.
OKAMOTO, K., ICHINOKAWA, T. & OHTSUKI, Y. (1971). *J. Phys. Soc. Jpn*, **30**, 1690-1700.
PENNYCOOK, S. J. & BOATNER, L. A. (1988). *Nature (London)*, **336**, 565-567.
RADI, G. (1970). *Acta Cryst.* A**26**, 41-56.
REIMER, L. & FROMM, I. (1989). *Proc. 47th Ann. Meet. Electron Microscopy, Society of America*, edited by G. W. BAILEY, pp. 382-383. San Francisco Press.
REZ, P., HUMPHREYS, C. J. & WHELAN, M. J. (1977). *Philos. Mag.* **35**, 81-96.
ROSSOUW, C. J. & BURSILL, L. A. (1985). *Acta Cryst.* A**41**, 320-328.
SPENCE, J. C. H. (1988). *Experimental High-Resolution Electron Microscopy* 2nd ed., p. 128. Oxford Univ. Press.
SPENCE, J. C. H. & SPARGO, A. E. (1971). *Phys. Rev. Lett.* **26**, 895-898.
TAKAGI, S. (1958). *J. Phys. Soc. Jpn*, **13**, 278-286.
WANG, Z. L. (1989). *Acta Cryst.* A**45**, 636-645.
WANG, Z. L. (1990). *Phys. Rev. B*, **41**, 12818-12837.
WANG, Z. L. (1991). *Philos. Mag.* Submitted.
WANG, Z. L. & BENTLEY, J. (1990). *Proc.* XII *Int. Congr. for Electron Microscopy, Seattle*, Vol. 2, edited by L. D. PEACHEY & D. B. WILLIAMS, pp. 532-533. San Francisco Press.
WANG, Z. L. & BENTLEY, J. (1991*a*). *Ultramicroscopy*. In the press.
WANG, Z. L. & BENTLEY, J. (1991*b*). *Miscrosc. Microstruct. Microanal.* Submitted.
WANG, Z. L. & COWLEY, J. M. (1990). *Ultramicroscopy*, **32**, 275-289.
WHELAN, M. J. (1965*a*). *J. Appl. Phys.* **36**, 2099-2102.
WHELAN, M. J. (1965*b*). *J. Appl. Phys.* **36**, 2103-2110.
XU, P., KIRKLAND, E. J., SILCOX, J. & KEYSE, R. (1990). *Ultramicroscopy*, **32**, 93-102.
YOSHIOKA, H. (1957). *J. Phys. Soc. Jpn*, **12**, 618-628.

Acta Cryst. (1991). A**47**, 698-702

About the Treatment of Weak Reflexions in Direct Procedures

BY G. CASCARANO, C. GIACOVAZZO AND A. GUAGLIARDI

Istituto di Ricerca per lo Sviluppo di Metodologie Cristallografiche, c/o Dipartimento Geomineralogico, Campus Universitario, 70124 *Bari, Italy*

(*Received* 6 *December* 1990; *accepted* 19 *April* 1991)

Abstract

Measurement of weak reflexions is often skipped by computer-controlled diffractometers. Such a practice can cause systematic errors in the scale and thermal factors as calculated by a Wilson plot, with consequent difficulties for the solution of the crystal structure by direct methods. A simple statistical method for estimating unobserved reflexions is described together with applications of the method.

1. Abbreviations

N number of atoms in the unit cell
s $(\sin\theta)/\lambda$
B overall thermal factor
K absolute scale factor
f_j^0 scattering factor of jth atom at rest
f_j scattering factor of jth atom, thermal vibration included
F structure factor

$$\sum\nolimits_o = \sum_{j=1}^{N} f_j^{02}$$

$$\sum = \sum_{j=1}^{N} f_j^2$$

n_o number of different observed reflexions in a shell of the Wilson plot (symmetry equivalents and/or Friedel pairs included)
n_u number of different unobserved reflexions in a shell (symmetry equivalent and/or Friedel pairs included)

$$n_t = n_o + n_u$$

$$I = |F_{\rm obs}|^2$$

I_M threshold intensity for unobserved reflexions in a given range of the Wilson plot
z normalized value of I
z_M threshold value of z for unobserved reflexions in a given range of the Wilson plot.

2. Introduction

Reflexions with intensity below a certain threshold are often considered as 'unobserved', *i.e.* their measurement is skipped by computer-controlled diffractometers. There are practical reasons for this: time is saved in data collection and crystal radiation damage is reduced. But there are also some drawbacks:

(*a*) The structural information contained in such weak reflexions is neglected. This may be vitally

0108-7673/91/060698-05$03.00